· Article · Advances in Polar Science
doi: 10.12429/j.advps.2024.0022 December 2024 Vol. 35 No. 4: 459-472

Sustainable observations of landfast sea ice in the cryosphere: a case study at the Liaodong Bay, Bohai Sea, North China

MA Yuxian[1], WANG Qingkai[2], LIU Xueqin[1], LI Wei[3*], XU Ning[1] & Bin CHENG[4]

[1] National Marine Environmental Monitoring Center, Dalian 116023, China;
[2] State Key Laboratory of Coastal and Offshore Engineering, Dalian University of Technology, Dalian 116024, China;
[3] State Key Laboratory of Nonlinear Mechanics, Institute of Mechanics, Chinese Academy of Sciences, Beijing 100190, China;
[4] Finnish Meteorological Institute (FMI), Helsinki FI-00101, Finland

Received 24 July 2024; accepted 6 November 2024; published online 30 December 2024

Abstract Sustainable monitoring of sea ice is crucial for better understanding air-ice-ocean interactions and identifying new processes. However, it is an expensive process particularly for the polar cryosphere environment. The seasonal ice-covered sea area can be used as a test bed for cryosphere-related process studies due to convenient access and conduction of field work, and the seasonal regime variation of the Arctic sea ice resulting from climate changes. In this paper, a small landfast sea ice monitoring program has been carried out for four consecutive seasons at Jiangjunshi Port, the Bohai Sea, North China, analyzing the temperature and salinity of air, ice and ocean and discussing the influence on mechanical properties. The effect of air temperature on sea ice temperature is focused. During low-temperature periods, the maximum correlation coefficient between air temperature and ice temperature, along with temperature fluctuation within ice, decreases as ice depth increases. Ice salinity was measured using ice core sampling and ice crumb sampling, with ice crumb salinity twice larger compared to ice core sampling when the ice temperature is −3 ℃. Ice salinity variations with ice temperature and the salinity profiles were fitted. Analysis of the profiles of under-ice seawater salinity reveals the presence of a high-salinity layer near the bottom of sea ice during the initial stage of sea ice growth. Based on the dynamic changes in sea ice temperature and sea ice salinity, this study evaluates the mechanical properties of sea ice, with the fitting determination coefficients of the obtained parameterized formulas significantly better than those reported in current research.

Keywords **seasonal sea ice**, **thermodynamic observations**, **sea ice temperature**, **sea ice salinity**, **uniaxial compressive strength**

Citation: Ma Y X, Wang Q K, Liu X Q, et al. Sustainable observations of landfast sea ice in the cryosphere: a case study at the Liaodong Bay, Bohai Sea, North China. Adv Polar Sci, 2024, 35(4): 459-472, doi: 10.12429/j.advps.2024.0022

1 Introduction

Sea ice is a crucial oceanographic condition in high-latitude regions such as polar and subpolar regions, and changes in ice conditions serve as an integrated indicator of global climate change. Due to harsh environmental conditions, effective and continuous collection of in-situ observation data in polar regions exhibits difficulties, which restricts the accuracy of

* Corresponding author. ORCID: 0000-0002-8348-2185. E-mail: liwei@imech.ac.cn

forecasts in polar meteorology and climate (Wang et al., 2022a; Webster et al., 2022).

Due to climate warming, the Arctic is warming nearly 4 times faster than the global average (Rantanen et al., 2022). Arctic studies have also indicated sea ice thickness's regime shift (Sumata et al., 2023). From the oceanography point of view, there is evidence that the impact of the Atlantic warm water on the Arctic Ocean has been intensified (Polyakov et al., 2023), and a so-called Atlantification of the Arctic Ocean is seen. As a result, there is a potential risk that the majority of the Arctic sea ice regime would shift from multi-year sea ice floes to the seasonal sea ice floes. The existence length of seasonal sea ice cover is also gradually shortened. The thinning and seasonality of Arctic sea ice would potentially narrow the difference between sea ice in the Arctic Ocean and seasonal ice-covered seas, such as the Baltic Sea and the Bohai Sea (Granskog et al., 2006; Ma et al., 2024; Vihma and Haapala, 2009; Yan et al., 2020)

The seasonal ice-covered sea can be used as a test bed for cryosphere-related process studies due to the relatively convenient access and conduction of field work and the seasonal regime variation of the Arctic sea ice resulting from climate changes (Garcia-Soto et al., 2021). By observing sea ice in the Bohai Sea, we can compensate for the lack of observations of polar sea ice in the context of climate change. We can also provide field data for validating remote sensing algorithms and numerical models, revealing the patterns of changes in polar sea ice and its interactions with the climate system. Therefore, fully utilizing the valuable sea ice in the Bohai Sea and conducting in-depth observations and research are of great significance for advancing the development of polar science (Cheng et al., 2021).

The observation of sea ice in the Bohai Sea is profoundly influenced by dynamic factors that cause sea ice dragging and accumulation (Liu et al., 2022; Zhang et al., 2020), resulting in a relative lack of research on fast ice. This situation is primarily caused by two reasons. Firstly, the thickness of sea ice in the Bohai Sea is relatively small (Ma et al., 2023; Zhang et al., 2021), and the survival period of the same piece of sea ice is significantly low (Wang et al., 2021), making it impractical to use expensive disposable drifting buoys for long-term and effective observations. Secondly, due to the complex dynamic environment of the Bohai Sea (Yan et al., 2022), selecting an appropriate test site for observation is exceptionally difficult. Considering the above factors, the observation of the thermodynamic process finds it challenging to the research. In January 2023, R/V *Zhong Shan Da Xue Ji Di* conducted cruise observations in the Bohai Sea. Due to the time limit, observations of the internal properties of sea ice were not performed. Therefore, we need to investigate new observation technologies and methods and seek to carry out "air-ice-ocean" observations on fast ice to gain more comprehensive knowledge of the characteristics of sea ice in the Bohai Sea.

The temperature and salinity of sea ice are fundamental for assessing its intrinsic properties (Kawano and Ohashi, 2009; Notz, 2005) and determining the parameters of remote sensing imagery (Segal et al., 2020; Yan et al., 2020). Influenced by meteorological and hydrological factors, however, the lack of continuous observation data on sea ice temperature and salinity results in a severe scarcity of studies on the physical and mechanical properties of seasonal sea ice. This situation not only leads to an inadequate description of the conditions and characteristics of seasonal sea ice, but also results in a shortage of necessary observational data for sea ice numerical simulations (Eicken, 2003; Lei et al., 2010; Neufeld and Wettlaufer, 2008). Taking the mechanical properties of sea ice as an example, current research often fails to fully consider the impact of dynamic changes in sea ice's physical properties on sea ice's mechanical properties (Golden et al., 1998; Ji et al., 2020; Schwarz and Weeks, 1977).

We have developed and integrated economical and practical observation equipment in the Bohai Sea and proposed a method for observing sea ice salinity. We have conducted winter sea ice observations for four consecutive years at Jiangjunshi Port on the east coast of Liaodong Bay in the Bohai Sea. Notably, during the observation in 2020/2021, we successfully collected crucial information, such as meteorological data, sea ice's temperature and salinity, and under-ice seawater salinity. Unfortunately, no fast ice formed at Jiangjunshi Port in the winters of 2021/2022 and 2022/2023, and our observations were limited to meteorological elements. But in the winter of 2023/2024, we successfully gained meteorological data once again, and based on observations of sea ice temperature and salinity, further collected field observation data on the mechanical properties of sea ice. According to these observations, this paper will delve into the observation methods of the sea ice in the Bohai Sea, elaborate on the inter-annual characteristics of sea ice conditions, analyze the interactions between meteorology, sea ice, and seawater, and accurately describe the properties of sea ice's uniaxial compressive strength.

2 Methods

2.1 Research area

Considering the motion characteristics of flat ice, we were faced with the challenge of selecting an appropriate test site with fast ice when conducting continuous and simultaneous "air-ice-ocean" observations on single-layer sea ice in the Bohai Sea. To address these issues, in this paper, we selected Jiangjunshi Port (on the east coast of Liaodong Bay, North China) as the experimental site after thorough field investigations for the areas with severe ice conditions in the Bohai Sea. Jiangjunshi Port is located at

39°55′7.72″N, 121°40′40.77″E, with its observation location shown in Figure 1. This site not only complies with the conditions of open sea but also, to the maximum extent possible, is free of aerodynamic and hydrodynamic forces. Inside Jiangjunshi Port, there is a small harbor with an area of approximately 1.6×10^5 m^2 and a depth of water of 8 m. In winter, the harbor basin is easily covered by fast ice, thereby being a natural experimental site for studying the thermodynamic mechanisms of sea ice growth and melt in the Bohai Sea.

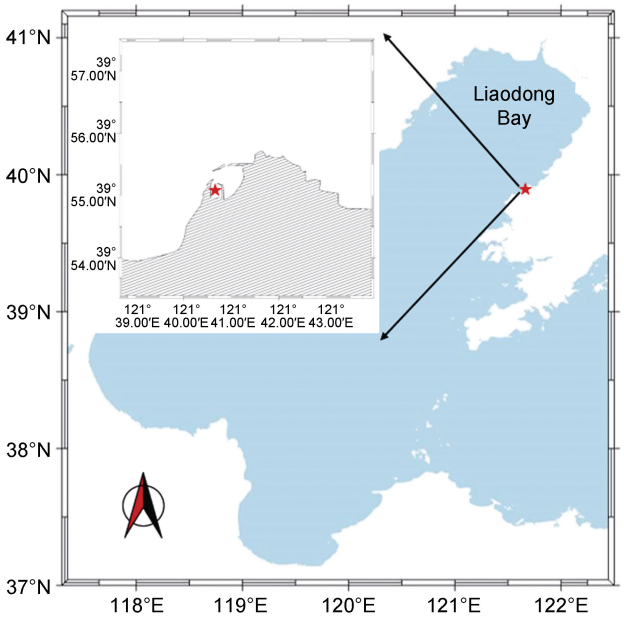

Figure 1 Coastline near Jiangjunshi Port.

2.2 Observation methods

Affected by ocean dynamic factors, the risk of flat ice movement with ocean currents in the Bohai Sea is significantly higher than that in other sea areas, potentially causing the loss of observation equipment for measuring the temperature and salinity of sea ice and seawater in the Bohai Sea. Furthermore, the thickness of fast ice in the Bohai Sea is much smaller than that in other sea areas, making it challenging to apply profile observation equipment suitable for other sea areas to the Bohai Sea. Therefore, the above issues highlight the necessity to develop economical and practical observation equipment.

Meteorological observation was mainly conducted with an automatic weather station equipped with Maximet GMX500, an integrated meteorological sensor. This sensor can observe multiple meteorological elements, including air temperature, wind speed, wind direction, humidity, and air pressure. The sensor's parameters are as follows: wind speed resolution 0.01 $m\cdot s^{-1}$; wind direction resolution 1°; humidity resolution 1%; temperature resolution 0.1 ℃; and air pressure observation resolution 0.1 hPa. Additionally, the observation frequency of this sensor was set to once every 5 s, ensuring real-time and accurate collection of data.

For the observation of sea ice temperature, we chose MEACON (http://www.meaconauto.com/) pt100 thermal resistor as the sensor, with an accuracy of 0.1 ℃ and a temperature measurement range of −50 to 200 ℃. Before use, we strictly calibrated the sensors to unify their readings at 0 ℃. The data collected by the sensor was aggregated through a collector and could be stored locally or wirelessly transmitted in real-time using a DTU (https://www.usr.cn/Product/cat-112.html). This allowed the data to be uploaded directly to a cloud server or transmitted to a computer in the laboratory via a network port. Finally, we fixed the sensor on the sea ice profile. Compared to materials such as PVC and metal, wood strip is advantageously featured by low thermal conductivity and ease in processing, thereby being used for enclosing the sensor for protection in this study.

Two methods were adopted for collecting sea ice salinity. First, the general method for measuring sea ice salinity was used. After sampled, the ice cores were immediately cut into 8 cm segments along the thickness of ice and then bottled for melting indoors. Subsequently, the sea ice salinity of each section was measured using a salinity meter. However, this method could result in salt loss during sampling (Gough et al., 2012; Massonnet et al., 2018; Vancoppenolle et al., 2009). Therefore, this paper used another approach, an in-situ observation method for sea ice salinity (Ma et al., 2024). To distinguish the above two sampling methods, the former is herein referred to as "ice core salinity sampling" and the latter as "ice crumb salinity sampling".

For the observation of seawater temperature and salinity, we chose the KZY-KO-LAEG temperature sensor (https://www.bjklzd.com/gyyl/133.html) and the SAL/CON5000 salinity sensor (https://www.nbchao.com/p/10257/). The temperature sensor was sealed with glue, with a measurement range of −20 ℃ to 86 ℃ and an accuracy of ±0.2% of the sensor range. The temperature sensor was powered by a 24 V power and output a 4–20 mA two-wire current signal. In addition, the salinity sensor was used to measure changes in electrical conductivity and salinity values in aqueous systems. At the site, the data collectors at each monitoring point were connected via a 485 bus "hand-in-hand", and the terminal data collector was connected to a RS485 to RS232 addressable conversion module. This module used a RS232 to USB cable to access an onshore computer without a network.

The sea ice mechanics test was mainly conducted with a hydraulic sea ice press. To ensure the comparability of test results, we strictly followed the recommendations of the International Association for Hydraulic Research (IAHR) and standardized the production process of test samples (Dong et al., 2023; Wang et al., 2023). According to the dimension recommended by IAHR, the sample used for the uniaxial compressive strength test was 7 cm×7 cm×17.5 cm

and was precisely re-measured before the experiment to ensure the accurate dimension of the sample (Paul et al., 2023; Xiu et al., 2022). Prior to sea ice sampling, the salinity and density of sea ice were also measured.

The schematic diagram for synchronous observation of "air-ice-ocean" is shown in Figure 2. Along the thickness of sea ice, sea ice temperature was measured using a digital temperature thermistor. The temperature observation was done jointly with hydraulic sea ice press experiments. We further categorized ice temperature into every 5 cm interval up to 8 layers. Similarly, we divided the sea ice salinity into 6 layers (8, 16, 24, 32, 40, and 48 cm) with a step size of 8 cm and measured the average salinity of each layer. The collection and measurement of salinity were conducted using the YSI 556MPS multi-parameter water quality meter with a measurement accuracy of 0.01. Before measurement, we calibrated the equipment using standard seawater. The ice conditions at the observation site are shown in Figure 3.

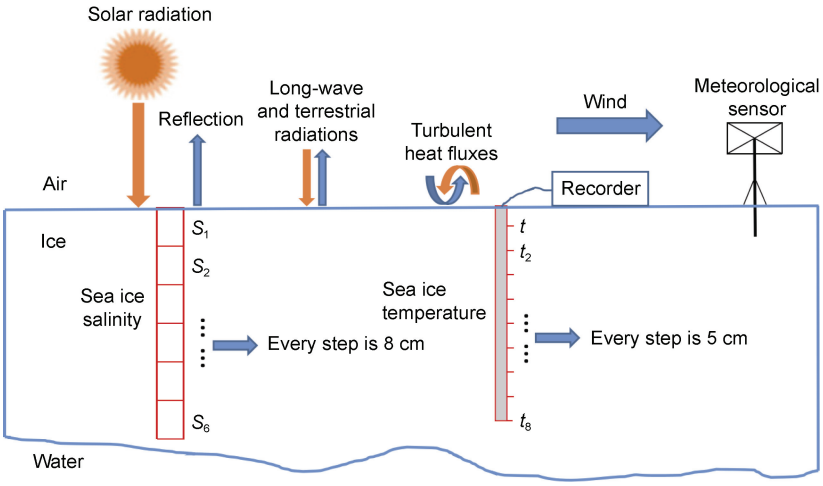

Figure 2 Schematic diagram of field air-ice-ocean synchronous observation.

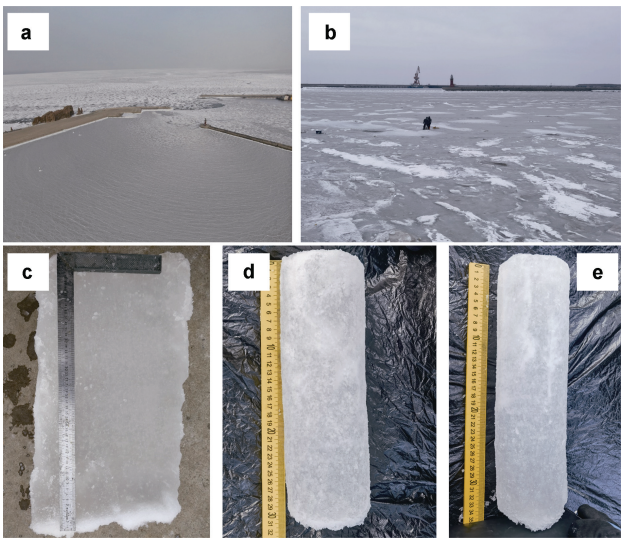

Figure 3 The experimental area off the Jiangjunshi Port. **a**, a bird view of the observation site, the camera facing NNW direction on 1 February 2021; **b**, in-situ measurement of sea ice thickness on 2 February 2024. The camera was facing the NNE direction. The ice thickness was 32 cm, and the surface was mostly snow-free, but occasionally snow patches were seen; **c**–**e**, ice core samples collected on 26 January 2021 (H_i = 51 cm), 1 February 2024 (H_i = 31 cm) and 5 February 2024 (H_i = 35 cm), respectively.

2.3 Data analysis method

When analyzing the relationship between the air temperature and the ice temperature profile, we employed the cross-correlation analysis method (Ghazani and Khosravi, 2020). Specifically designed to measure the correlation between two time-series datasets, this method determines the degree of correlation and temporal sequence of the two datasets by thoroughly analyzing the similarity of the two datasets under different time lags. In cross-correlation analysis, we shifted one dataset relative to the other in terms of time to find the best matching point (the position with the highest correlation). This method can help us uncover potential correlations between the two datasets (Werneck et al., 2024), such as interactions between climate variables and correlations in price variations of the financial market.

For the analysis of sea ice temperature and sea ice salinity, we employed a fitting method based on the least squares method. The least squares method is a mathematical optimization technique widely used in data analysis, statistical learning, and signal processing (Tang et al., 2022). This method focuses on finding a function that minimizes the sum of the squares of the deviations (residuals) between the function and the data points (Wu et al., 2021). This method can help us extract helpful information from complex datasets and describe the overall trend of the data through a simple mathematical model (Kono and Sato, 2021). According to the characteristics of the data, we can practically choose different functions for fitting, such as linear functions and polynomial functions, to better reveal the inherent relationships between datasets (Soto-Quiros, 2022).

3 Results

3.1 Spatiotemporal distribution characteristics

The spatiotemporal distribution of sea ice conditions in the Bohai Sea exhibits significant inter-annual variations. Over the past four winters, landfast ice didn't survive a long time enough during winters 2021/2022 and 2022/2023 in the Jiangjunshi Port test site. The landfast ice formed on site around 20 January, 2022, but soon broke up due to warm air temperature and resulted in a few sporadic floating ice floes by 14 February, 2022. From 15 to 25 February, 2022, the landfast ice froze up again after a major cold air outbreak with a large air temperature drop. However, the ice thickness is not thick enough to qualify for the operation safety criteria and ice samples were not available unfortunately. At the time when ice existed, the solar radiation was strong and further weakened the ice and ice cover soon disappeared completely after 25 February, 2022. For winter 2022/2023, no large stable ice cover was ever formed, but only scattered sea ice floes appeared near the port because extremely warm air temperature was observed in early January when it was usually the best time for ice formation at the observation site. Apart from the above two winters, landfast ice existed for 36 d in the winter of 2020/2021 and for 19 d in the winter of 2023/2024. To comprehensively understand the characteristics of sea ice in the Bohai Sea, in the winter of 2020/2021, we conducted on-site observations of meteorological conditions, sea ice temperature, sea ice salinity, and under-ice seawater temperature and salinity, which required a longer observation period. In the winter of 2023/2024, we tested the mechanical properties of sea ice based on on-site observations of sea ice temperature and salinity.

3.1.1 Meteorological observation results

Meteorological conditions fundamentally drive the inter-annual variations in the severity of ice conditions in the Bohai Sea. Empirically, the severity of sea ice conditions in the Bohai Sea can be assessed by the air temperatures pattern from 25 December to 15 February (D25F15). Our in-depth analysis of temperature data during this period (D25F15) shows significant seasonal variations in the 4 winter seasons' average air temperatures (Figure 4a). The mean air temperature during this period for these 4 seasons were −3.0 ℃ (2020/2021), −2.6 ℃ (2021/2022), −1.9 ℃ (2022/2023) and −2.8 ℃ (2023/2024), respectively.

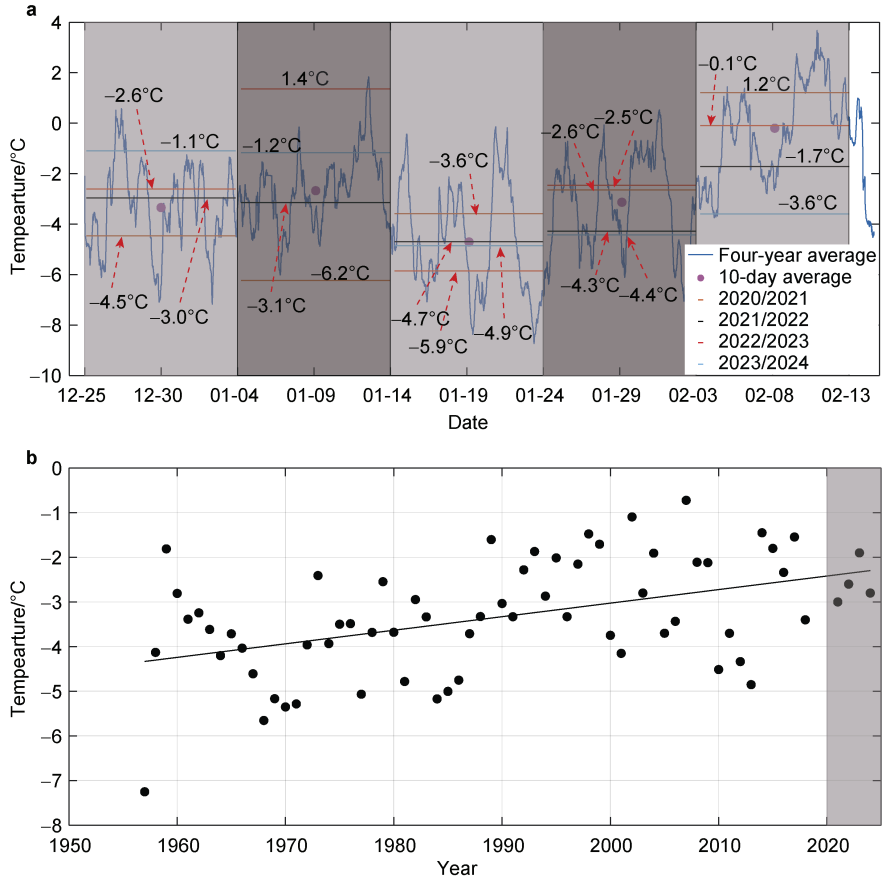

Figure 4 **a**, time series of average air temperature for 4 winter seasons (blue line). The horizontal bars are 10-day average air temperature for each season. **b**, multi-decadal (1957–2018) winter seasonal mean air temperature observed at Wafangdian weather station, 20 km to the observation site. The fitting line is generated by using the Theil-Sen estimator. The grey column marks recent 4 seasons.

Specifically, the winter of 2020/2021 exhibits the lowest average temperature followed by the winter of 2023/2024. In contrast, the average winter temperatures in 2021/2022 and 2022/2023 are higher, with 2 warm winters in the past four years. The interannual variability of air temperature during D25F15 around the Bohai Sea is the basic driving force determining the severity of Bohai Sea landfast ice condition (Ma et al., 2022). The severity of ice condition for each individual winter season is mainly constrained by two factors: the average seasonal air temperature and the length of low air temperature accumulated from cold air outbreaks. The greater the drop in average air temperature, and the more frequent and intense cold air outbreaks, the more severe landfast sea ice conditions will be. Compared with the winter of 2021/2022 and 2023/2024, although the difference in average air temperature during D25F15 was only −0.2 ℃, the longer interval between the cold outbreaks and warmer mean air temperature in early winter (Figure 4a) makes the ice conditions in that season significantly lower than in 2023/2024. The interannual variation of mean air temperature observed by a weather station close to the observation site suggested a clear warm trend (Figure 4b), with a temperature increase rate of 0.03 ℃·a^{-1} ($p < 0.05$). The variability of seasonal mean air temperature was consistent with the observed ice condition on site.

3.1.2 Sea ice temperature profiles

Regarding continuous observations on temperature profiles of sea ice in the Bohai Sea, a thermistor string hourly measurements of about 8 d in the vicinity of Bayuquan (on the east coast of Liaodong Bay) in the 1990s was a good example. The data collection was part of the long-term Finnish-Chinese sea ice collaboration (Cheng, 2002; Leppäranta et al., 2021). However, one limitation of this observation is that the sea ice's thickness only increased from 32 cm to 38 cm during the observation, thus failing to cover the sea ice with rapid growth under a warming process and at high temperatures.

In this section, to delve into the characteristics of ice temperature profiles at low values, rising values, and continuously high values, we selected three typical periods (8–9, 18–21, and 25–28, January 2021) as case studies to conduct detailed ice temperature profile analysis. Prior to the ice temperature analysis, we first averaged the ice temperatures for these three time periods to eliminate the influence of ice temperature fluctuations. The results of the ice temperature profile analysis are shown in Figure 5. For the period of low air temperatures (8–9 January), the sea ice temperature profile exhibits a linear pattern, indicating that heat is rapidly contacted away from the bottom of the sea ice and resulting in ice growth at the bottom. For the warm up stage (18–21 January), as air temperature rises, the upper ice layer warms faster than ice bottom. The temperature gradient was weakened at the lower ice layer; the ice growth slowed down. A striking finding was a peak of the in-ice temperature below the surface. This warm up is due to the solar heating. For the warming period (25–28 January), the sea ice temperature profile exhibits a coexistence of high temperatures at the 10 cm position and low temperatures at the 15 cm position. Notably, during warmup stage a cold intermediate layer was seen. The low temperature appeared at the 15 cm position below the surface.

The salient characteristics of the vertical profile of sea ice temperature include the "subsurface-layer high temperature" and "cold intermediate layer". The formation of the "cold intermediate layer" is mainly due to the strong heat exchange between the sea ice surface and the atmosphere, and the heat dissipation efficiency of the sea ice in this layer is significantly reduced. The "subsurface-layer high temperature" is mainly due to the influence of solar shortwave radiation, which is very different from the origin of the "cold intermediate layer". The main factor contributing to this phenomenon is the intense solar radiation at low latitudes, which leads to the formation of a distinct high-temperature layer between the ice surface and the "cold intermediate layer" of the sea ice. In addition, sea ice temperature fluctuates intensely on the ice surface, which is also caused by diurnal variations of solar radiation.

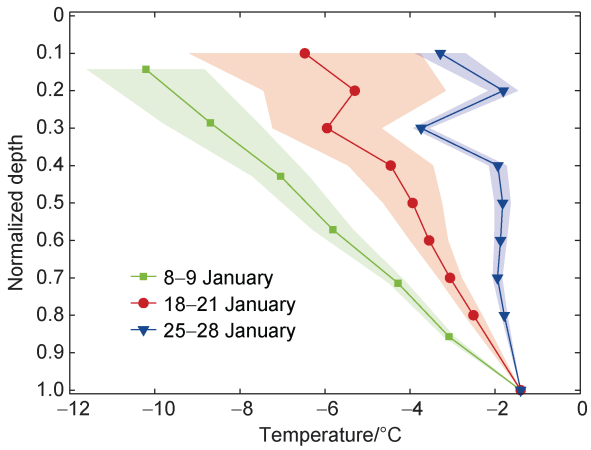

Figure 5 Temperature profiles measured by the thermistor string. Three scenarios were represented, i.e. cold condition, 8–9 January, 2021; warm up stage, 18–21 January and rising-temperature; and warming period, 25–28 January. The solid lines with symbol are the mean vertical in-ice temperature during each condition. The shading areas are corresponding to the mean square deviation (MSD) of the temperature profiles in each stage.

3.1.3 Sea ice salinity profiles

In the past, sea ice salinity was primarily sampled with the ice core sampling method, but this method was often accompanied by significant loss of brine during the sampling process, especially at the ice-ocean interface (Gough et al., 2012; Li and Fedorov, 2021). Additionally, current studies on sea ice salinity are limited by discontinuous spatiotemporal sampling, providing most

analyses with discrete data points (Vancoppenolle et al., 2009). To address this issue, this study used a sampling method for ice crumb salinity in addition to the observations of ice core salinity. During the winter of 2020/2021, we sampled 11 sets of ice core salinity and 16 sets of ice crumb salinity at Jiangjunshi Port, with 8 sets of data collected using both methods simultaneously. During the sampling process, the thickness of the sea ice remained 48 cm.

Firstly, we analyzed the profile characteristics of ice core salinity. From 21 to 27 January, 2021 when the sea ice temperature remained relatively high, the sea ice exhibited a higher salinity only in the bottom layer, showing a typical "L"-shaped distribution pattern. From 29 to 30 January when the sea ice temperature decreased, the sea ice salinity profile showed a "C"-shaped distribution. After 2 February when the sea ice temperature continued to drop, the mid-layer sea ice salinity remained at 4 to 5 psu, while the bottom-layer salinity basically remained at 5 to 7 psu.

Secondly, we analyzed the profile characteristics of ice crumb salinity. On 16 January, 2021 when the sea ice temperature remained low, and the ice crumb salinity exhibited an inverse "C"-shaped distribution. From 17 to 19 January when the sea ice temperature gradually decreased, the ice crumb salinity profile turned to a "C"-shaped distribution compared to the previous pattern of increasing from top to bottom. However, after 17:00 on 19 January, when most sea ice temperatures remained above −6 ℃, the ice crumb salinity profile generally showed a pattern of increasing gradually from top to bottom.

Finally, we analyzed the differences between ice crumb salinity and ice core salinity. When the sea ice temperature was relatively low, the profiles of both ice core salinity and ice crumb salinity exhibited similar "C"-shaped distribution patterns. However, when the sea ice temperature rose, differences became prominent between the two salinities: The ice crumb salinity profile showed a pattern of increasing gradually from bottom to top, while the ice core salinity exhibited an "L"-shaped distribution with higher values in the bottom layer and relatively uniform values at other positions. To quantify the differences between ice crumb salinity and ice core salinity, we studied the variations between the two salinities (Figure 6). These results indicate a clear positive correlation between the sea ice salinity variations and sea ice temperatures. This means that as the sea ice temperature rose, the differences between ice crumb salinity and ice core salinity also increased gradually.

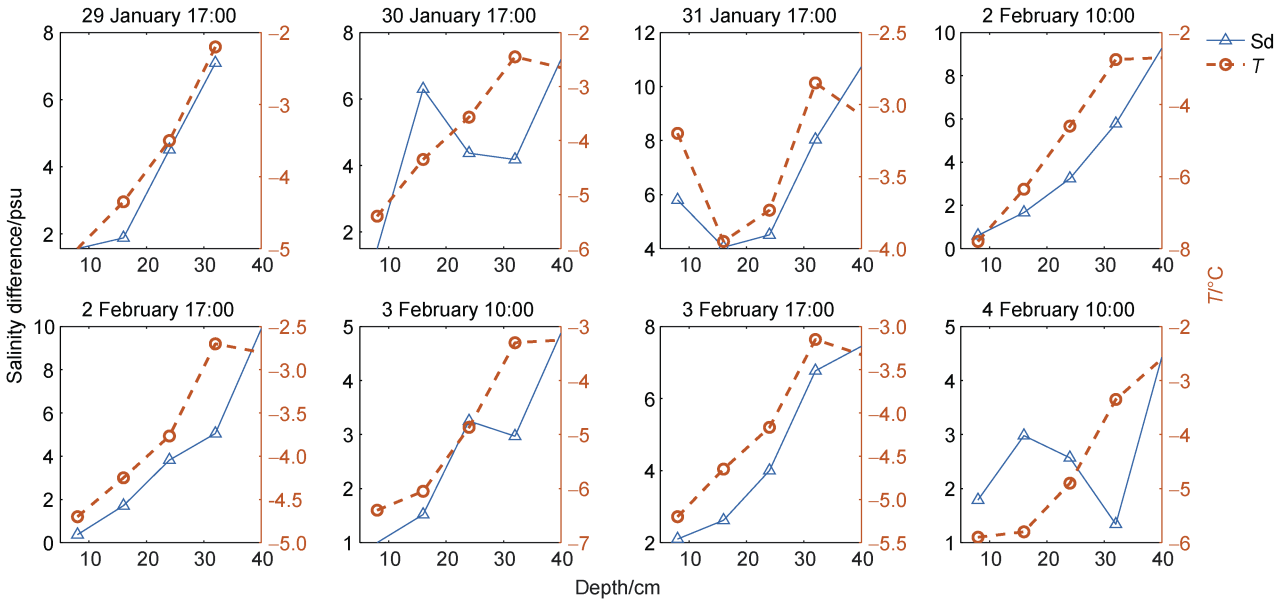

Figure 6 Variation of salinity difference (Sd) profile and sea ice temperature (T) profile.

The vertical variation pattern of sea ice salinity is crucial for solving the thermal balance equation of internal ice (Morland, 1984; Raymond, 2000). To ensure the accuracy of the results and minimize the impact of data fluctuations, the salinity data on the vertical profile was averaged in this study. Subsequently, the least squares method was used to fit and analyze the processed average salinity data.

The average salinity data of the profile sampled from the ice core exhibits a typical "C"-shaped distribution; the temperature range of those ice samples was between −8 to −1.8 ℃. Specifically, the average salinity remains at 4.1 to 4.7 psu for a depth of 0 to 40 cm and increases to 5.8 psu for a depth of 40 to 48 cm. The fitting result of the profile is

$$S_{\mathrm{co}}(h) = a \times \mathrm{e}^{b \times h} + c \times \mathrm{e}^{d \times h} \quad (1)$$

where, h represents the normalized ice thickness, 0 for the ice surface and 1 for the ice bottom; a = 4.71, with a 95% confidence interval of 4.85 to 4.57; b = −0.17, with a 95% confidence interval of −0.09 to −0.24; c = 0.00001, with a 95% confidence interval of 0.0001 to −0.00001; d = 12.05,

with a 95% confidence interval of 16.30 to 7.79; R^2 represents the coefficient of determination, 0.99.

The average salinity data of the profile sampled from the ice crumb shows a gradual increase from the surface to the bottom. Specifically, the average ice crumb salinity gradually increases from 8.5 psu at the surface to 14.2 psu at the bottom. The profile fitting formula is:

$$S_{\mathrm{cr}}(h) = a \times \mathrm{e}^{b \times h} + c \times e^{d \times h} \quad (2)$$

where, h represents the normalized ice thickness, 0 for the ice surface and 1 for the ice bottom; a = 7.58, with a 95% confidence interval of 10.53 to 4.63; b =−0.51, with a 95% confidence interval of 1.71 to −2.72; c = 0.96, with a 95% confidence interval of 5.10 to −3.18; d = 2.31, with a 95% confidence interval of 5.45 to −0.83; R^2 represents the coefficient of determination, 0.99.

Last, we studied the spatial differences between ice core salinity and ice crumb salinity. The results show that the average salinity variation gradually increases from 1.9 to 7.8 psu from the sea ice surface to the bottom, indicating significant differences in the spatial distribution of ice core salinity and ice crumb salinity.

3.1.4 Seawater salinity profiles

The salinity variations of under-ice seawater are directly influenced by the processes of sea ice growth and melt. Disturbed by atmospheric conditions, energy is transferred through the sea ice to the under-ice seawater. At the same time, variations of the energy inside the sea ice can also lead to the release of salts within the ice, further resulting in dynamic changes in the salinity of under-ice seawater. Therefore, this section focuses on discussing the variations in the salinity of under-ice seawater.

Figure 7 illustrates the variation pattern of under-ice seawater salinity throughout the ice season. According to our analysis of the patterns of seawater salinity, there are significant differences in seawater salinity at different spatial locations. In the early ice season, the seawater salinity near the bottom of the ice was close to 37 psu, significantly higher than that at other locations.

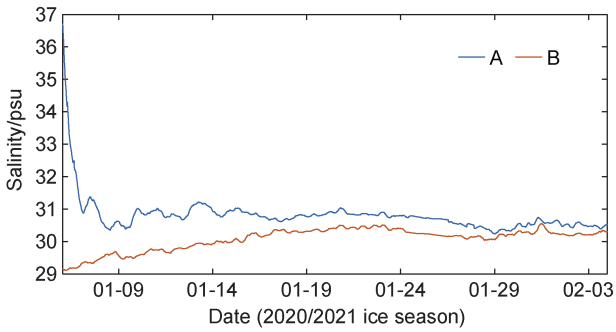

Figure 7 Salinities throughout the ice season: A and B represent the salinity at 0.9 m and 2.0 m below the ice surface, respectively.

During the growth and melt of sea ice, the seawater salinity is directly influenced by the thermal processes of sea ice. In the early sea ice growth, the rapid growth of sea ice led to the rapid release of salts, which is the main reason for the peak salinity of under-ice seawater. Subsequently, as the seawater mixed, the salinities tended to coincide with each other.

3.2 The relationship between air temperature and ice temperature

The correlation between air temperature and ice temperature is significant. To analyze the pattern of ice temperature response to changes in air temperature, this study selected air temperature and ice temperature series during low-temperature periods (7–13 January, 2021) and high-temperature periods (22–28 January, 2021). Using cross-correlation analysis (with a step size of 0.5 h), we calculated the lag time of ice temperature changes relative to air temperature changes, with the results shown in Table 1.

Table 1 The lag time of ice temperature relative to air temperature and the maximum correlation coefficient

Standard ice thickness	Low-temperature periods		High-temperature periods	
	Maximum correlation coefficient	Lag time/min	Maximum correlation coefficient	Lag time/min
0.05	0.880	110	0.302	1320
0.15	0.897	130	0.318	1410
0.25	0.900	160	0.262	1540
0.35	0.901	200	0.123	2010
0.45	0.903	220		
0.55	0.902	230		
0.65	0.876	230		
0.75	0.829	230		
0.85	0.768	310		
0.95	0.738	310		

Note: Standardized ice thickness refers to the ratio of ice thickness at the temperature measurement point to the total ice thickness.

During low-temperature periods, the maximum correlation coefficient between ice temperature and air temperature decreases as the depth increases. This is because the position closer to the upper surface of sea ice will be increasingly influenced by air temperature, posing a higher sensitivity of ice temperature to air temperature. In the middle part of sea ice, the sensitivity of ice temperature to air temperature gradually decreases due to the "filtering" effect of the upper part on air temperature and the gradual influence of the lower heat source (seawater) on the middle part. Affected by the stable water temperature, with the entire ice layer undergoing brine changes and heat consumption due to sea ice temperature changes, the lower part of sea ice has a low correlation between ice temperature and air temperature. The lag time corresponding to the maximum correlation coefficient increases with depth. During high-temperature periods, the correlation between air temperature and ice temperature

only exists when the standard ice thickness is less than 0.35, with a maximum correlation coefficient of 0.302 and a minimum lag time of 1320 min.

3.3 The relationship between sea ice temperature and sea ice salinity

There is a close relationship between sea ice temperature and sea ice salinity. As detailed above, sea ice temperature directly affects the phase equilibrium between internal brine and pure ice. Meanwhile, the variation pattern of sea ice salinity to sea ice temperature is also essential for solving the sea ice energy balance equation. Therefore, we need to explore the relationship between sea ice temperature and sea ice salinity.

3.3.1 The relationship between ice core salinity and sea ice temperature

The salinity of sea ice in the Bohai Sea is mainly determined by the brine within brine pockets and brine channels. During the sampling process of ice core salinity, the seawater in brine channels within the ice will directly drain away. Therefore, ice core salinity mainly represents the salt level of brine pockets within the ice, while ice crumb salinity reflects the sum of salt in brine pockets and brine channels. The difference between the two salinities can indicate the content of brine in brine channels.

To understand the impact of sea ice temperature on ice core salinity, this paper illustrates the relationship between sea ice temperature and ice core salinity (Figure 8). According to the observations, sea ice salinity exhibits a decrease in sea ice temperatures from −7 to −2.5 ℃, with a fitting formula of S=−0.14×T+3.92 (p<0.05). However, when sea ice temperature exceeds −2.5 ℃, sea ice salinity begins to increase, with a fitting formula of S=1.87×T+8.73 (p<0.05).

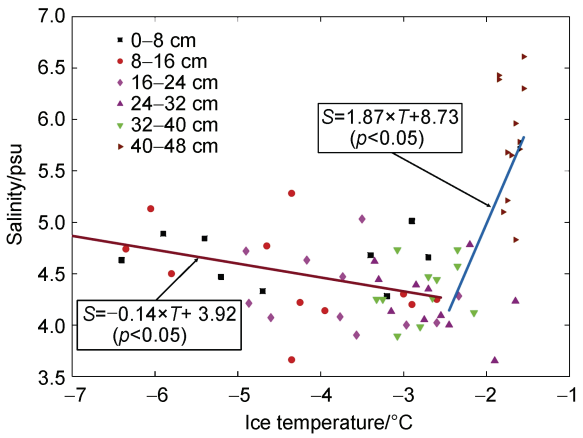

Figure 8 Scatter plot of ice core salinity and ice temperature.

The dynamic changes in the pore within sea ice under varying sea ice temperatures are the main reasons for the above laws. Brine pockets gradually convert into brine channels with the increase in sea ice temperature, and the loss of brine occurs during the sampling process, leading to a decrease in the salinity of the sea ice core. When the sea ice temperature exceeds −2.5 ℃ and continues to rise, the salinity of the sea ice sample increases at its bottom (40–48 cm). This is because the ice bottom always contacts the seawater, and the brine released by gravity from the upper open brine cells also passes through the ice bottom.

3.3.2 The relationship between ice crumb salinity and sea ice temperature

Ice crumb salinity is considered the sum of the salinity of brine pockets and brine channels within the ice and can indicate the true content of brine within the ice in a more accurate manner compared to ice core salinity. To demonstrate the changes in brine content within the ice as ice temperature varies, this paper has established the relationship between ice crumb salinity and ice temperature (Figure 9). When the ice temperature is below −5 ℃, the sea ice salinity remains at approximately 8 psu. As the sea ice temperature gradually rises, the ice crumb salinity also begins to increase gradually, showing an ever-increasing growth rate. The relationship between ice crumb salinity and ice temperature is fitted as S=51.88×T/(2.71+3.86×T−0.74×T^2−0.05×T^3), applicable to −8 to −1.8 ℃ (p < 0.05).

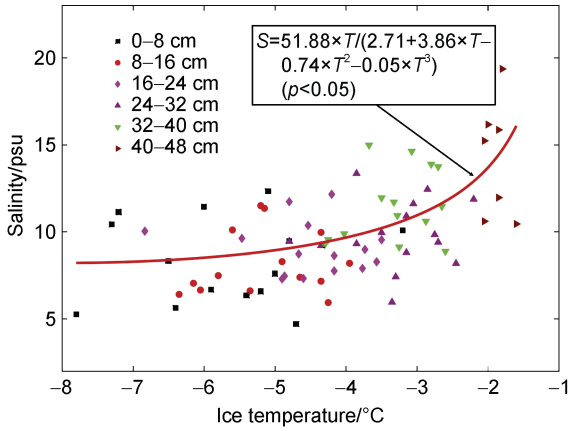

Figure 9 Scatter plot of ice crumb salinity and ice temperature.

3.3.3 The relationship between brine content in brine channels and sea ice temperature

The variation between ice crumb salinity and ice core salinity is defined as the brine content in brine channels within the sea ice, namely, the loss of brine (salinity difference) during ice core sampling. Figure 10 illustrates the changes in the content of brine in brine channels with ice temperature. As the sea ice temperature rises, salinity difference also exhibits a steady increase. Specially, the variation between ice crumb salinity and ice core salinity is approximately 1 psu at an ice temperature of −8 ℃; however, when the ice temperature rises to −3 ℃, this variation increases to 6 psu, and the data distribution is more scattered. To further elucidate the relationship between salt loss and ice temperature, this paper fitted their

relationship and derived a parameterized formula:

$$y=a\times e^{b\times T} \quad (3)$$

where, a = 20.2, with a 95% confidence interval from 10.35 to 30.05; b = 0.415, with a 95% confidence interval from 0.26 to 0.57; T represents the temperature of sea ice (℃), with a range of −8 to −2 ℃.

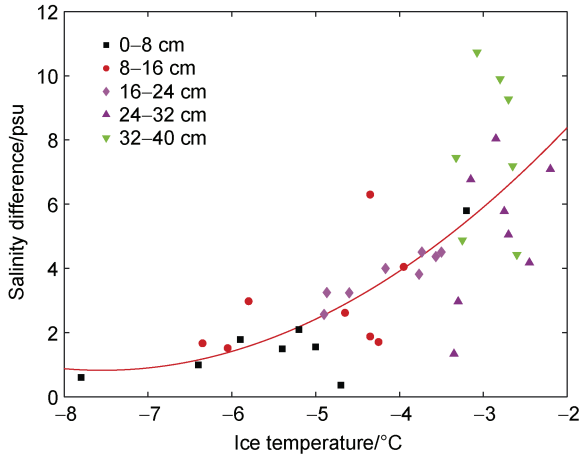

Figure 10 Variation of salinity difference with ice temperature.

3.4 The relationship between brine volume fraction and sea ice compressive strength

The salinity and temperature of sea ice determines the ratio of pure ice to brine within the ice. Due to different properties of liquid and solid phases, the properties of sea ice are largely dependent on the brine volume fraction within sea ice. Generally, brine pockets and brine channels are considered as natural damage points in sea ice, so the brine volume fraction has been regarded as a key parameter for evaluating the mechanical strength of sea ice.

During the winter of 2023/2024, the uniaxial compressive strength of sea ice was measured based on field observations of sea ice temperature and salinity (Figure 11). The average temperatures of the sea ice samples in the test were −7.8, −5.9, −4.3, and −2.9 ℃, respectively. Given the significant impact of loading rate on the mechanical properties of sea ice, we chose a strain rate (10^{-3}·s^{-1}) within the "ductile-brittle" transition zone for loading and adopted horizontal loading (Riska, 2018). During the test, we assumed that the internal structures of the samples were similar.

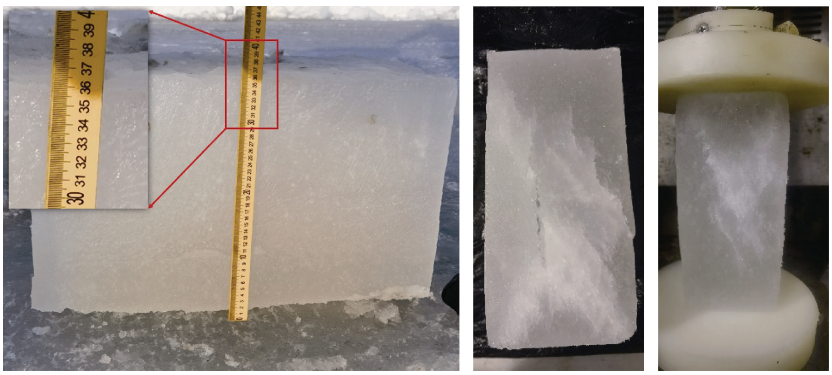

Figure 11 Compression test of sea ice at Jiangjunshi Port.

When sampling sea ice for mechanical test, sea ice temperature (T) and sea ice salinity (S) were recorded at the sampling location. After processed, the ice sample was recorded with its densities, thereby deriving the brine volume fraction (v_b) of the sea ice sample:

$$v_b = \frac{\rho \times S}{F_1} \quad (4)$$

$$F_1(T) = -4.732-22.45\times T-0.6397\times T^2-0.01074\times T^3 \quad (-22.9\leqslant T\leqslant -2\ ℃) \quad (5)$$

$$F_1(T) = -0.041221-18.407\times T+0.58402\times T^2+0.21454\times T^3 \quad (T>-2\ ℃) \quad (6)$$

where, ρ is sea ice density (g·cm^{-3}); S is the sea ice salinity (psu); T is sea ice temperature (℃); F_1 is an empirical function of ice temperature (g·cm^{-3}).

Eq. (5) is given by Cox and Weeks (1983) and Eq. (6) is by Leppäranta and Manninen (1988).

The relationship between the uniaxial compression of sea ice and brine volume fraction is expressed in an exponential function and a power function (e.g., Ji et al., 2020; Timco and Weeks, 2010; Wang et al., 2022b), respectively:

$$\sigma = \alpha \times e^{\beta\sqrt{v_b}} \quad (7)$$

$$\sigma = \alpha\left(\sqrt{v_b}\right)^{\beta} \quad (8)$$

where, α and β are fitting parameters. The fitting results are shown in Table 2. Figure 12 presents the fitting results when the strain rate is 10^{-3}·s^{-1}. Despite merely 15 datasets, the fitting results are significantly better than those reported (Wang et al., 2016). One possible explanation could be linked with the timing of the experiments. As far as we know, uniaxial compression experiments have been largely carried out in the cold laboratory where the temperature was tuned artificially. Under such circumstances, the v_b of the ice sample may differ considerably compared

with that of the newly collected ice sample on site. In this study, all the uniaxial compression experiments have been carried out on site. As a result, the v_b is more representative in reflecting the actual physical properties of sea ice, which leads to a better agreement between data and parameterization function.

Table 2 Fitting parameters for the relationship between uniaxial compressive strength and square root of brine volume fraction

Function	α	β	R^2	SSE	RMSE
Exponential function	14.56	−6.99	0.81	3.41	0.46
Power function	0.24	−1.67	0.82	3.15	0.44

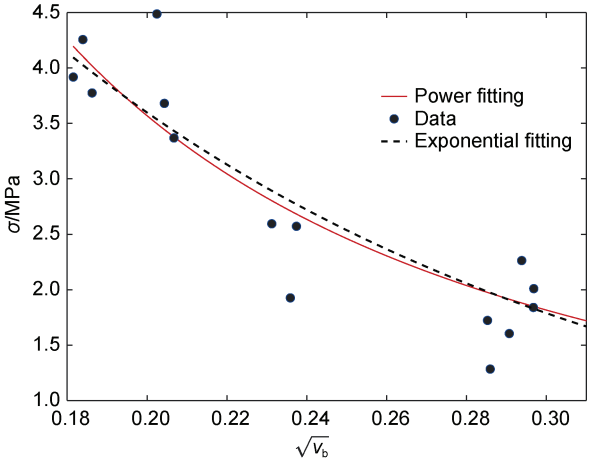

Figure 12 The exponential and power fitting functions of sea ice strengths with $\sqrt{v_b}$.

4 Discussion

Restricted by dynamic factors, there lack continuous "air-ice-ocean" observations of fast ice throughout the ice period in the Bohai Sea. To address this issue, we have integrated observation equipment, proposed a new observation method, and conducted "air-ice-ocean" observations at Jiangjunshi Port on the east coast of the Liaodong Bay, China for four consecutive years, aiming to investigate the inter-annual variation of ice conditions and analyze the interactions between air, ice, and ocean.

Meteorological conditions serve as the core driving force for the growth and melt of sea ice in the Bohai Sea, and the inter-annual variation of meteorological conditions leads to fluctuations in the severity of ice conditions in the Bohai Sea (Su et al., 2012; Ouyang et al., 2019). Over the past four winters, the average winter temperatures, from lowest to highest, are in the order of 2020/2021, 2023/2024, 2021/2022, and 2022/2023, with the severity of ice conditions following the same pattern. Meanwhile, high-frequency changes in air temperature directly affect the fluctuations in sea ice temperature. During low-temperature periods, air temperature and ice temperature are correlated; during high-temperature periods, however, the correlation between air temperature and ice temperature is not significant. Furthermore, the lag time of sea ice temperature relative to air temperature gradually increases from the ice's upper surface to the bottom.

In response to the current brine loss during sea ice core sampling, this paper used a method for sampling ice crumb salinity to avoid brine loss (Ma et al., 2024). According to the observations and analysis, ice core salinity and ice crumb salinity exhibit differences in their spatial variation patterns. Specially, the average value of ice core salinity at each depth presents a "C"-shaped distribution from top to bottom (Li and Sui, 1989; Li et al., 1991, 1992), similar to historical observation results in the Bohai Sea and the salinity profiles of seasonal sea ice in polar regions, while the average value of ice crumb salinity gradually increases from top to bottom at each depth. To quantitatively describe the spatial patterns of brine loss during the sampling process, this paper analyzed the average variations between ice crumb salinity and ice core salinity at various depths, indicating that the content of brine loss gradually increases from the surface to the bottom, with a maximum average loss of 7.8 psu. After fitting the data with profile averages, this paper presented parameterized formulas on vertical profiles for ice core salinity and ice crumb salinity, with their coefficients of determination of 0.99.

Ice core salinity and ice crumb salinity can characterize the brine volume in brine pockets and brine channels within the sea ice in the Bohai Sea, while sea ice temperature directly affects the dynamic balance between ice phase and water phase. As sea ice temperature gradually decreases, brine channels will shrink or even disappear compressed by surrounding ice crystals, trapping the brine within the ice crystals with the salinity of the brine channels remaining at approximately 1 psu. However, when sea ice temperature starts to rise, brine pockets begin to expand and gradually blend themselves with the seawater at the bottom of ice, thereby shaping brine channels. If brine channels increase and widen, ice core salinity decreases; otherwise, ice crumb salinity starts to rise, and the salinity of the brine channels gradually climbs from 1 to 4 psu. Particularly, when sea ice temperature exceeds −2.5 ℃ and continues to rise, the brine channels within the ice will further increase and widen, leading to a sharp increase in both ice core salinity and ice crumb salinity with the salinity gap between them increasing from 4 to 10 psu.

The variation pattern of under-ice seawater salinity during the ice period is influenced by the interaction between sea ice salinity and temperature. In the early stage of sea ice growth, seawater salinity near the ice layer shows a significant increase, with an observed maximum seawater salinity of 36.8 psu; as sea ice thickness gradually remains stable, seawater salinity near the bottom of the ice gradually decreases to 30 psu.

The complexity of sea ice mechanical properties is determined by the dynamic processes of sea ice temperature

and salinity (Huang et al., 2021; Skatulla et al., 2022). Measurements of sea ice mechanical properties, based on simultaneous observations of sea ice temperature and salinity, can provide a more accurate description of the mechanical properties of sea ice. This paper has obtained a parameterized formula for the uniaxial compressive strength of sea ice under a strain rate of 10^{-3} in the "ductile-brittle" transition zone, with a fit determination coefficient greater than 0.8, much higher than other currently reported fitting results.

Although we have achieved simultaneous "air-ice-ocean" observations in the Bohai Sea, continuous observations are still needed to collect more effective data due to the inter-annual variation in the severity of ice conditions. Furthermore, we still need to confront the limitations of ice crumb salinity sampling method, despite its significant advantages compared to the ice core sampling method. Specially, ice crumb salinity sampling, similar to ice core salinity sampling, is also a destructive method, making it impossible to conduct continuous salinity observations on the same piece of sea ice. In addition, ice crumb salinity sampling can cover most sea ice temperatures, but when the temperature reaches the freezing point, the seawater may overflow during the ice crumb sampling near the bottom of the ice, thereby preventing ice crumb salinity observations from covering the entire temperature range of sea ice.

The ice crystal structure affects sea ice mechanical properties (Cox et al., 1985; Richter and Cox, 1985; Timco and Weeks, 2010). In this study the ice samples were collected in the level landfast ice zone where the ice was formed relatively quickly and uniformly, so the impact of ice crystal structure on sea ice mechanical properties was omitted. To evaluate the comprehensive mechanical properties of the Bohai sea ice, the ice crystal structure observation is needed.

In future, it is necessary to develop new sampling methods and increase the number of samples for in-situ sea ice salinity observations, aiming to enable studies on the interaction between sea ice temperature and sea ice salinity under the influence of meteorological conditions and to further clarify the variation patterns of physical and mechanical properties of sea ice.

5 Conclusion

This study has investigated the complicated interaction between meteorological conditions, seawater conditions, sea ice thermodynamics, and sea ice mechanical properties in the Bohai Sea, where the inter-annual variation of sea ice conditions exhibits significant fluctuations. Our findings reveal that the severity of sea ice conditions is directly driven by meteorological factors, with air temperature playing a dominant role in regulating sea ice temperature during the low-temperature periods. This highlights the importance of atmospheric factors in adjusting the thermodynamic balance between the atmosphere, sea ice, and under-ice seawater.

Notably, the study uncovers distinct patterns in sea ice salinity, with a "C"-shaped profile observed using ice core methods and a pattern of increasing from top to bottom for ice crumb. As sea ice temperature rises, these distinctive salinity patterns highlight the complexity of salt dynamics within sea ice. Furthermore, the initial period of sea ice growth is marked by salt release, producing a high-salinity layer in the under-ice seawater, which further complicates the thermodynamic and mechanical properties of sea ice.

These findings fundamentally contribute to understanding the physical and mechanical complexities of sea ice and lay a crucial data foundation for predicting sea ice evolution and its impacts under a changing climate. The investigation into the interaction between sea ice temperature and sea ice salinity highlights the fundamental reasons for the complexities of sea ice's physical and mechanical properties. Specifically, Previous studies did not consider the microscopic changes caused by the interactions between sea ice temperature and sea ice salinity in pressure tests, due to which the maximum fitting determination coefficient was only 0.51 (Wang et al., 2016) in the analysis of the mechanical strength variation with its brine volume fraction. In contrast, after the temperature-salinity interaction of sea ice was taken into account in mechanical tests carried out directly in the field, the maximum fitting determination coefficient in this paper increased to 0.82 according to the results of pressure tests.

To enhance our predictive capabilities and deepen our understanding of sea ice behaviors, it is imperative to conduct extensive field observations. Supplementing the existing dataset with additional measurements will not only refine models but also enable more accurate assessments of sea ice dynamics and their implications for regional and global climate systems.

Acknowledgement This work was financially supported by the National Natural Science Foundation of China (Grant nos. 42206221 and 42077445), Academy of Finland under contract 31799. We are grateful to two anonymous reviewers and Guest Editor Dr. Yinke Dou for their constructive comments that help to improve further this article.

Note This paper is a solicited article of Special Issue entitled "Novel technologies for sustainable monitoring of polar environment upscaling from in situ observations to aerial and space-borne remote sensing" published on Vol. 35 No. 3 in September 2024.

References

Cheng B, Vihma T, Palo T, et al. 2021. Observation and modelling of snow and sea ice mass balance and its sensitivity to atmospheric forcing during spring and summer 2007 in the Central Arctic. Adv Polar Sci, 32(4): 312-326, doi: 10.13679/j.advps.2021.0047.

Cheng B. 2002. On modelling ice thermodynamics and air-ice coupling of

the Bohai Sea and the Baltic Sea.. Ph.D thesis, Helsinki: Finnish Institute of Marine Research, 1-38. https://helda.helsinki.fi/items/6a42f387-b223-443a-a450-e0198055a015.

Cox G F N, Weeks W F. 1983. Equations for determining the gas and brine volumes in sea-ice samples. J Glaciol, 29(102): 306-316, doi:10.1017/s0022143000008364.

Cox G F N, Richter-Menge J A, Weeks W F, et al. 1985. Mechanical properties of multiyear sea ice, Phase II: test results. Hanover: CRREL Report 85-16.

Dong C, Luo X, Nie H, et al. 2023. Effect of compressive strength on the performance of the NEMO-LIM model in Arctic sea ice simulation. J Oceanol Limnol, 41(1): 1-16, doi:10.1007/s00343-022-1241-z.

Eicken H. 2003. From the microscopic to the macroscopic to the regional scale: growth, microstructure and properties of sea ice//Thomas D N, Dieckmann G S. Sea ice—an introduction to its physics, chemistry, biology and geology. Blackwell: Wiley-Blackwell, 22-81, doi:10.1002/9780470757161.ch2.

Garcia-Soto C, Cheng L J, Caesar L, et al. 2021. An overview of ocean climate change indicators: sea surface temperature, ocean heat content, ocean pH, dissolved oxygen concentration, Arctic sea ice extent, thickness and volume, sea level and strength of the AMOC (Atlantic meridional overturning circulation). Front Mar Sci, 8: 642372, doi:10.3389/fmars.2021.642372.

Ghazani M M, Khosravi R. 2020. Multifractal detrended cross-correlation analysis on benchmark cryptocurrencies and crude oil prices. Phys A Stat Mech Appl, 560: 125172, doi:10.1016/j.physa.2020.125172.

Golden K M, Ackley S F, Lytle V I. 1998. The percolation phase transition in sea ice. Science, 282(5397): 2238-2241, doi:10.1126/science.282.5397.2238.

Gough A J, Mahoney A R, Langhorne P J, et al. 2012. Sea ice salinity and structure: a winter time series of salinity and its distribution. J Geophys Res, 117(C3): C03008, doi:10.1029/2011jc007527.

Granskog M, Kaartokallio H, Kuosa H, et al. 2006. Sea ice in the Baltic Sea–a review. Estuar Coast Shelf Sci, 70(1/2): 145-160, doi:10.1016/j.ecss.2006.06.001.

Huang S, Huang M, Lyu Y, et al. 2021. Effect of sea ice on seismic collapse-resistance performance of wind turbine tower based on a simplified calculation model. Eng Struct, 227: 111426, doi:10.1016/j.engstruct.2020.111426.

Ji S, Chen X, Wang A. 2020. Influence of the loading direction on the uniaxial compressive strength of sea ice based on field measurements. Ann Glaciol, 61(82): 86-96, doi:10.1017/aog.2020.14.

Kawano Y, Ohashi T. 2009. A mesoscopic numerical study of sea ice crystal growth and texture development. Cold Reg Sci Technol, 57(1): 39-48, doi:10.1016/j.coldregions.2009.02.001.

Kono S, Sato M. 2023. The potentials of partial least squares structural equation modeling (PLS-SEM) in leisure research. J Leis Res, 54(3): 309-329, doi:10.1080/00222216.2022.2066492.

Lei R, Li Z, Cheng B, et al. 2010. Annual cycle of landfast sea ice in Prydz Bay, East Antarctica. J Geophys Res, 115(C2): C02006, doi:10.1029/2008jc005223.

Leppäranta M, Manninen T. 1988.The brine and gas content of sea ice with attention to low salinities and high temperatures. Finnish Institute of Marine Research Internal Report.

Leppäranta M, Vihma T, Cheng B, et al. 2021. An outstanding example of cooperation between Arctic and non-Arctic countries in cryosphere and climate research: Sino-Finnish cooperation for more than 30 years. Adv Polar Sci, 32(4): 261-263, doi: 10.13679/j.advps.2021.0088.

Li H, Fedorov A V. 2021. Persistent freshening of the Arctic Ocean and changes in the North Atlantic salinity caused by Arctic sea ice decline. Clim Dyn, 57(11): 2995-3013, doi:10.1007/s00382-021-05850-5.

Li Z, Sui J. 1989. Temperature salinity and density profiles in a fast ice sheet in Liaodong Bay//Port and Ocean Engineering under Arctic Conditions. Luleå: Luleå University of Technology, 66-72.

Li Z, Sui J, Dong X. 1991. Preliminary statistics of some sea ice conditions in Liaodong Gulf. Ocean Eng, 10(2): 72-78.

Li Z, Yang D, Meng G, et al. 1992. Relation of thermal conductivity coefficient with temperature of sea ice in Bohai Sea//Proceedings of the International Conference on Offshore Mechanics and Arctic Engineering (Offshore Technology). New York: American Society of Mechanical Engineers, 329-333.

Liu S, Liu S, Li G, et al. 2022. Impacts of sea ice on marine dynamics in western Laizhou Bay, Bohai Sea. Estuar Coast Shelf Sci, 275: 107958, doi:10.1016/j.ecss.2022.107958.

Ma Y, Cheng B, Leppäranta M, et al. 2024. Temperature and salinity in the Bohai Sea landfast ice: Observations and modelling. Cold Reg Sci Technol, 221: 104154, doi:10.1016/j.coldregions.2024.104154.

Ma Y, Cheng B, Xu N, et al. 2022. Long-term ice conditions in Yingkou, a coastal region northeast of the Bohai Sea, between 1951/1952 and 2017/2018: modeling and observations. Remote Sens, 14(1): 182, doi:10.3390/rs14010182.

Ma Y, Ding D, Xu N, et al. 2023. Ice mass balance in Liaodong Bay: modeling and observations. Water, 15(5): 943, doi:10.3390/w15050943.

Massonnet F, Vancoppenolle M, Goosse H, et al. 2018. Arctic sea-ice change tied to its mean state through thermodynamic processes. Nat Clim Change, 8: 599-603, doi:10.1038/s41558-018-0204-z.

Morland L W. 1984. Thermomechanical balances of ice sheet flows. Geophys Astrophys Fluid Dyn, 29(1-4): 237-266, doi:10.1080/03091928408248191.

Neufeld J A, Wettlaufer J S. 2008. An experimental study of shear-enhanced convection in a mushy layer. J Fluid Mech, 612: 363-385, doi:10.1017/s0022112008003339.

Notz D. 2005. Thermodynamic and fluid-dynamical processes in sea ice. Doctor dissertation, Cambridge: University of Cambridge, 87-93.

Ouyang L, Hui F, Zhu L, et al. 2019. The spatiotemporal patterns of sea ice in the Bohai Sea during the winter seasons of 2000–2016. Int J Digit Earth, 12(8): 893-909, doi:10.1080/17538947.2017.1365957.

Paul F, Schwarz C, Audh R, et al. 2023. Sea ice mechanics. Comput Methods Mater Sci, 23(3): 5-54, doi:10.7494/cmms.2023.3.0816.

Polyakov I V, Ingvaldsen R B, Pnyushkov A V, et al. 2023. Fluctuating Atlantic inflows modulate Arctic atlantification. Science, 381(6661): 972-979, doi:10.1126/science.adh5158.

Rantanen M, Karpechko A Y, Lipponen A, et al. 2022. The Arctic has warmed nearly four times faster than the globe since 1979. Commun Earth Environ, 3: 168, doi:10.1038/s43247-022-00498-3.

Raymond C F. 2000. Energy balance of ice streams. J Glaciol, 46(155): 665-674.

Richter J A, Cox G F N. 1985. A preliminary examination of the effect of structure on the compressive strength of ice samples from multi-year pressure ridges. J Energy Resour Technol, 107(1): 99-102, doi:10.1115/1.3231170.

Riska K. 2018. Ice edge failure process and modelling ice pressure. Phil

Trans R Soc A, 376(2129): 20170340, doi:10.1098/rsta.2017.0340.

Schwarz J, Weeks W F. 1977. Engineering properties of sea ice. J Glaciol, 19(81): 499-531, doi:10.3189/s0022143000029476.

Segal R A, Scharien R K, Cafarella S, et al. 2020. Characterizing winter landfast sea-ice surface roughness in the Canadian Arctic Archipelago using Sentinel-1 synthetic aperture radar and the Multi-angle Imaging SpectroRadiometer. Ann Glaciol, 61(83): 284-298, doi:10.1017/aog.2020.48.

Skatulla S, Audh R R, Cook A, et al. 2022. Physical and mechanical properties of winter first-year ice in the Antarctic marginal ice zone along the Good Hope Line. Cryosphere, 16(7): 2899-2925, doi:10.5194/tc-16-2899-2022.

Soto-Quiros P. 2022. A regularized alternating least-squares method for minimizing a sum of squared euclidean norms with rank constraint. J Appl Math, 2022, 4838182, doi:10.1155/2022/4838182.

Su H, Wang Y, Yang J. 2012. Monitoring the spatiotemporal evolution of sea ice in the Bohai Sea in the 2009–2010 winter combining MODIS and meteorological data. Estuaries Coasts, 35(1): 281-291, doi:10.1007/s12237-011-9425-3.

Sumata H, de Steur L, Divine D V, et al. 2023. Regime shift in Arctic Ocean sea ice thickness. Nature, 615(7952): 443-449, doi:10.1038/s41586-022-05686-x.

Tang Z, Zhang Z, Xu Z, et al. 2022. Load identification with regularized total least-squares method. J Vib Contr, 28(21/22): 3058-3069, doi:10.1177/10775463211024819.

Timco G W, Weeks W F. 2010. A review of the engineering properties of sea ice. Cold Reg Sci Technol, 60(2): 107-129, doi:10.1016/j.coldregions.2009.10.003.

Vancoppenolle M, Fichefet T, Goosse H, et al. 2009. Simulating the mass balance and salinity of Arctic and Antarctic sea ice. 1. Model description and validation. Ocean Model, 27(1/2): 33-53, doi:10.1016/j.ocemod.2008.10.005.

Vihma T, Haapala J. 2009. Geophysics of sea ice in the Baltic Sea: a review. Prog Oceanogr, 80(3/4): 129-148, doi:10.1016/j.pocean.2009.02.002.

Wang A, Xu N, Bi X, et al. 2016. Unified representation of sea ice strengths under influences of brine volume and stress rate. Haiyang Xuebao, 38(9): 126-133, doi:10.3969/j.issn.0253-4193.2016.09.013 (in Chinese with English abstract).

Wang Q, Li Z, Lu P, et al. 2022b. Flexural and compressive strength of the landfast sea ice in the Prydz Bay, East Antarctic. Cryosphere, 16(5): 1941-1961, doi:10.5194/tc-16-1941-2022.

Wang Q, Liu Y, Lu P, et al. 2023. The porosity effect on the mechanical properties of summer sea ice in the Arctic. Cryosphere, 1-21, doi:10.5194/tc-2023-31, 2023.

Wang X, Liu Y, Key J R, et al. 2022a. A new perspective on four decades of changes in Arctic Sea ice from satellite observations. Remote Sens, 14(8): 1846, doi:10.3390/rs14081846.

Wang Z, Sun P, Wang L, et al. 2021. Monitoring sea ice in Liaodong Bay of Bohai Sea during the freezing period of 2017/2018 using sentinel-2 remote sensing data. J Spectrosc, 2021: 9974845, doi:10.1155/2021/9974845.

Webster M A, Rigor I, Wright N C. 2022. Observing Arctic sea ice. Oceanography, 35(3/4): 29-37.

Werneck L R, Jessup C, Brandenberger A, et al. 2024. Cross-correlation image analysis for real-time single particle tracking. Rev Sci Instrum, 95: 073708, doi:10.1063/5.0206405.

Wu D, Wang Y, CaoJ, et al. 2021. Least-squares reverse-time migration with sparsity constraints. J Geophys Eng, 18(2): 304-316, doi:10.1093/jge/gxab015.

Xiu Y, Li Z, Wang Q, et al. 2022. Experimental study on flexural strength and effective elastic modulus of granular ice in the Bohai Sea, China. Front Energy Res, 10: 970051, doi:10.3389/fenrg.2022.970051.

Yan Y, Gu W, Gierisch A M, et al. 2022. NEMO-Bohai 1.0: a high-resolution ocean and sea ice modelling system for the Bohai Sea, China. Geosci Model Dev, 15(3): 1269-1288, doi:10.5194/gmd-15-1269-2022.

Yan Y, Uotila P, Huang K, et al. 2020. Variability of sea ice area in the Bohai Sea from 1958 to 2015. Sci Total Environ, 709: 136164, doi:10.1016/j.scitotenv.2019.136164.

Zhang N, Li S, Wu Y, et al. 2020. Effects of sea ice on wave energy flux distribution in the Bohai Sea. Renew Energy, 162: 2330-2343, doi:10.1016/j.renene.2020.10.036.

Zhang Y, Hang S, Han Y, et al. 2021. Sea ice thickness detection using coastal BeiDou reflection setup in Bohai Bay. IEEE Geosci Remote Sensing Lett, 18(3): 381-385, doi:10.1109/LGRS.2020.2980106.